High resolution WENO simulation of 3D detonation waves

Cheng Wang[1], Chi-Wang Shu[2], Wenhu Han[3] and Jianguo Ning[4]

Abstract

In this paper, we develop a three-dimensional parallel solver using the fifth order high-resolution weighted essentially non-oscillatory (WENO) finite difference scheme to perform extensive simulation for three-dimensional gaseous detonations. A careful study is conducted for the propagation modes of the three-dimensional gaseous detonation wave-front structure in a long square duct with different widths under different initial perturbations. The numerical results indicate that, with a transverse sinusoidal perturbation of the initial ZND profile, when the width of the duct is less than the cellular width ($4.5\times L_{1/2}$), unstable detonations can trigger a spinning motion in the duct. The detonation wave propagates in a single-headed spinning motion, with a distinctive "ribbon" displayed on the four walls. In this case, the measured pitch-to-diameter ratio is approximately 3.42, which is slightly larger than the theoretically predicted value 3.128 for a round duct. When the channel width is greater than the cellular width, detonation waves propagate in an out-of-phase rectangular mode. With a transverse cosine perturbation of the initial ZND profile, the front of the stable detonation has a rectangular structure, and regular cellular patterns and in-phase "slapping waves" can be observed clearly on the four walls. The width-to-length ratio of the cellular patterns is approximately 0.5. For a mildly unstable detonation, its front has an in-phase rectangular structure at the early stage, then the wave-front becomes flat. Over time, but it still maintains an in-phase rectangular structure after reigniting. For highly unstable detonations, the wave-front has a rectangular structure at the early stage. After a low pressure stage for a very long time, detonation occurs once again. At this time, the detonation front structure becomes very twisted, and the triple-lines become asymmetrical. Finally, a spinning detonation mode is triggered. With a symmetrical perturbation mode along the diagonals of the detonation front, for the stable detonation, an diagonal detonation is formed and the detonation front maintains a diagonal structure, but no "slapping waves" appears on the walls. The width-to-length ratio of the cellular structure is equal to that in the rectangular structure. For mildly unstable and highly unstable detonations, the front has a diagonal structure at the early stage. After a short period of time, the diagonal structure of the detonation front cannot be maintained, and it ultimately evolves into a spinning detonation.

Keywords: high order WENO finite difference scheme; cellular structure; unstable detonation; spinning detonation; rectangular mode; diagonal mode

[1]State Key Laboratory of Explosion Science and Technology, Beijing Institute of Technology, Beijing, 100081, P.R. China. E-mail: wangcheng@bit.edu.cn.

[2]Division of Applied Mathematics, Brown University, Providence, RI 02912. E-mail: shu@dam.brown.edu.

[3]State Key Laboratory of Explosion Science and Technology, Beijing Institute of Technology, Beijing, 100081, P.R. China.

[4]State Key Laboratory of Explosion Science and Technology, Beijing Institute of Technology, Beijing, 100081, P.R. China. Email: jgning@bit.edu.cn.

1 Introduction

Detonation is a complex supersonic flow phenomenon where its front consists of a precursor shock wave that propagates into the unreacted medium at supersonic speed with a thin reaction zone immediately behind the shock. The precursor shock compresses the unreacted medium and increases its temperature. Burning occurs behind the front, which can release a large amount of heat that in turn supports the precursor shock wave to keep propagating forward.

Numerous experimental and numerical studies have been performed to study detonation. However, detailed numerical studies on detonation mostly remain in two-dimensional simulations. As is well known, detonation is essentially a three-dimensional phenomenon, and some important structural features cannot be obtained from two-dimensional simulations, such as the slapping waves and spinning structures. Unfortunately, a highly refined grid resolution is required for such computation, especially for unstable detonation, which makes three-dimensional numerical simulation of detonation tremendously computing-resource intensive. In this paper, we attempt to address this difficulty by developing a high order accurate weighted essentially non-oscillatory (WENO) solver with parallel implementation so that the desired wave structures can be resolved within acceptable computational time. WENO schemes have the advantage of high order accuracy and robust, sharp, and essentially non-oscillatory shock resolution [1, 2, 3, 4].

Previous research in the literature indicates that the heat of the reaction, the activation energy, the overdrive factor and the ratio of specific heat all have some effects on the stability of detonation and cellular patterns [5, 6]. Bourlioux et al. [7], Papalexandris et al. [8], He and Karagozian [9], and Daimon and Matsuo [10] carried out numerical simulation of one-dimensional detonations. Guirguis et al. [11], Bourlioux and Majda [12], Papalexandris et al. [13], Gamezo et al. [14], Hwang et al. [15], and Shepherd et al. [16] carried out numerical simulation of two-dimensional detonations. These numerical simulations have investigated the instability of the detonation in details and have drawn some very important

conclusions. The instability of the detonation wave leads to irregular cellular structure which is caused by transversely developing of triple points (triple lines in three-dimensional detonation waves) along the front. For unstable detonations, a very small initial perturbation will quickly develop transversely with time. Therefore, with different reactive parameters, such as the heat of reaction, the activation energy and the overdrive factor, and with a given initial perturbation and geometrical configuration, the detonation front structure may have different evolution processes, and hence the detonation modes may be different.

Detailed experimental study on three-dimensional gas detonation structure has been conducted as early as in the 1960s (White and Cary [17] and Strehlow [18]). Recent numerical simulations and experimental results have shown that there are three main types of cellular detonation structures, namely rectangular, diagonal, and spinning modes [19, 20]. Hanana et al. [21], by experimental study, pointed out that in rectangular tubes at least two types of detonation structure exist, namely the rectangular and diagonal structures. Through the soot-foil tracks on the walls, they showed the diamond-shaped cellular patterns. They also showed that the rectangular structure is characterized by straight triple lines emanating from the leading front that are parallel or orthogonal to the walls of the flow domain. Another characteristic feature is the occurrence of slapping waves on the walls. These waves are formed by collisions between a triple line and the wall or between two triple lines. They divided rectangular detonation modes into in-phase and out-of-phase. When a cluster of parallel triple lines collide with the walls simultaneously, an in-phase rectangular detonation is formed. On the contrary, it will be an out-of-phase rectangular detonation. When the movement direction of the triple-line is along the diagonal line, the detonation front has a diagonal structure, and the direction of the transverse wave propagation has a 45° angle with the wall, while on the wall the slapping waves would disappear. Further, they pointed out that, compared with a rectangular detonation, a diagonal detonation has a high front pressure, a large average velocity and a reduced cell length, and that the rectangular detonation formed by the overlapping of two two-dimensional detonations. However, in their

experimental research, they did not observe out-of-phase detonation. They believed the ignition method was the key factor for the formation of different detonation modes. However, they did not give the relationship between different detonation modes, the front features of different detonation modes and the mechanism of their generation. Williams et al. [22] adopted a one-step reaction model and performed numerical simulation of three-dimensional detonation in a rectangular duct, and observed the front rectangular structure. Tsuboi et al. [23] carried out three-dimensional numerical simulation of detonation propagation in the rectangular duct, and further confirmed the detonation is divided into in-phase rectangular and out-of-phase modes. Deledicque and Papalexandris [24] studied the rectangular and diagonal structures of detonations in a three-dimensional rectangular tube by using a one-step chemical reaction model. When the overdrive factor $f = 1.1$, the heat of reaction $Q = 2.0$, and the activation energy $Ea = 20$, the detonation is in a rectangular out-of-phase mode under the transverse sinusoidal perturbation, and out-of-phase "slapping waves" are formed on the walls which are mutually perpendicular in the square tube. When they used a constant perturbation along the diagonals of the front, a diagonal detonation was formed. They also studied the rectangular mode of the unstable detonation for the activation energy $Ea = 50$, the heat of reaction $Q = 50$, and the overdrive factors $f = 1.2$ and $f = 1.6$ under a sinusoidal perturbation, but they did not study the evolution of the two unstable detonation fronts in perturbation along the diagonals of the front.

Campbell and Woodhead [25] identified the phenomenon of spinning detonations in small-diameter tubes near the detonation limits. They found that the pitch of the spin is about three times the diameter of the pipe, see also [26]. Lee et al. [27] observed a single-headed spinning detonation in a square channel through the soot-foil record, and the single helical trajectory from the four side walls of the square channel is unfolded to show the same soot characteristics as in the round duct. Recently, studies have revealed more information on spinning detonation in rectangular channels and round tubes [23, 28, 29, 30, 31, 32, 33, 34, 35, 36]. Zhang et al. [26, 30] conducted experimental studies on the two-phase flow detonation

in a round tube, and showed that in a stable propagation of detonation, the transverse wave has played a leading role. Huang et al. [31] conducted experiments on spinning detonations with a detailed analysis of the shock structure. Experimental results indicate that the actual structure of the spinning detonation tries to match closely to the condition where the state parameters (pressure and temperature) reach their maximum values. Tsuboi and co-workers [23, 36, 37, 38] also carried out extensive numerical simulations on the detonation in round tubes and rectangular ducts. They pointed out that the formation of an unburned gas pocket behind the detonation front was not observed in their results because the rotating transverse detonation completely consumed the unburned gas. Dou et al. [39, 40] investigated spinning detonation in narrow channels and detonation structures under different initial perturbations by numerical simulation. Their numerical results showed that the spinning detonation only exists in narrow channels. When the channel width is large enough, the spinning detonation goes away. These studies on the spinning detonation do not consider modes of propagation of detonation waves in tubes of different widths or when different chemical reaction parameters are selected. Therefore, with different chemical reaction parameters, the dynamical behavior and spinning mechanism of the spinning detonation remain unclear, and whether a change in duct width and initial perturbation can trigger spinning detonation warrants further study.

The main objective of this paper is to simulate numerically the detonation modes in different square tubes, with different chemical reaction parameters and under different initial disturbances, to provide a detailed front structure description for each detonation mode and further to find out the conditions for triggering spinning detonation.

2 Governing equations

The governing equations are the three-dimensional Euler equations with a source term that represents chemical reactions. In conservation form, these equations may be written in the compact form

$$\frac{\partial U}{\partial t} + \frac{\partial F(U)}{\partial x} + \frac{\partial G(U)}{\partial y} + \frac{\partial H(U)}{\partial z} = S \tag{1}$$

where the conserved variable vector U, the flux vectors F, G, and H as well as the source term S are given, respectively, by

$$U = (\rho, \rho u, \rho v, \rho w, \rho E, \rho Y)^T \tag{2}$$

$$F(U) = (\rho u, \rho u^2 + p, \rho uv, \rho uw, \rho u(E + p/\rho), \rho uY)^T \tag{3}$$

$$G(U) = (\rho v, \rho vu, \rho v^2 + p, \rho vw, \rho v(E + p/\rho), \rho vY)^T \tag{4}$$

$$H(U) = (\rho w, \rho wu, \rho wv, \rho w^2 + p, \rho w(E + p/\rho), \rho wY)^T \tag{5}$$

$$S(U) = (0, 0, 0, 0, 0, \rho\omega)^T \tag{6}$$

$$E = \frac{RT}{\gamma - 1} + YQ + \frac{1}{2}(u^2 + v^2 + w^2) \tag{7}$$

$$\omega = -K\rho Y e^{-(Ea/RT)} \tag{8}$$

$$p = \rho RT \tag{9}$$

here u, v, w are the Cartesian components of the fluid velocity in the x, y, z directions, respectively, ρ is the density, p is the pressure, E is the total energy per unit volume, T is the temperature, and Y is the reactant mass fraction. Q is the heat of reaction, Ea is the activation energy, $\gamma = 1.2$ is the specific heat ratio, and K is the pre-exponential factor.

Zeldovich, von Neumann and Doring [41] sought the one-dimensional steady ZND analytical solution in the 1940s. When we specify the steady state solution in term of the dimensionless primitive variables in unreacted zone as $\rho = 1, P = 1, u = -D$, the ZND analytical solution can be given by the formula

$$\rho = \frac{D^2(\gamma - 1)}{-\gamma(D^2 + 1) + \xi(Y)(\gamma - 1)D} \tag{10}$$

$$u = \frac{-\gamma(D^2 + 1)}{(\gamma - 1)D} + \xi(Y) \tag{11}$$

$$P = \frac{-\gamma(D^2 + 1)}{\gamma - 1} + D\xi(Y) + D^2 + 1 \tag{12}$$

where

$$\xi(Y) = \sqrt{\gamma(D^2 + 1)^2/(\gamma + 1)D^2 - \frac{2(\gamma - 1)}{(\gamma + 1)}((1 - Y)Q + \frac{\gamma}{(\gamma - 1)} + 0.5D^2)} \tag{13}$$

and the detonation velocity $D^2 = (D_{CJ})^2 f$, with the overdrive factor $f \geq 1$, and D_{CJ} being the C-J detonation velocity, given as follows [20]

$$D_{CJ} = \sqrt{(\gamma^2 - 1)\, Q/2} + \sqrt{(\gamma^2 - 1)\, Q/2 + \gamma p_0/\rho_0}. \tag{14}$$

3 The numerical method

In this section we briefly describe the general framework of the the ($2r$-1)-th order local characteristics based weighted essentially non-oscillatory (WENO) conservative finite difference scheme for solving the system of hyperbolic conservation laws in Section 2. More details can be found in [2, 3]. In the subsequent computation we use the fifth order ($r = 3$) version.

Consider a uniform grid defined by the grid points $x_i = i\Delta x$, $i = 0, \cdots, n_x$, $y_j = j\Delta y$, $j = 0, \cdots, n_y$, and $z_k = k\Delta z$, $k = 0, \cdots, n_z$, where for simplicity $\Delta x = \Delta y = \Delta z$ is the uniform grid spacing. The cell boundaries are given by $x_{i+1/2} = x_i + \Delta x/2$, $y_{j+1/2} = y_j + \Delta y/2$, $z_{k+1/2} = z_k + \Delta z/2$. The original partial differential equation is written, at the grid points, in the following form

$$\frac{dU(x_i, y_j, z_k, t)}{dt} = \left(-\frac{\partial F(U)}{\partial x} - \frac{\partial G(U)}{\partial y} - \frac{\partial H(U)}{\partial z} + S \right) \Big|_{x=x_i, y=y_j, z=z_k} \tag{15}$$

A conservative finite difference scheme for approximating the equation (15) can be written as

$$\frac{dU_{i,j,k}}{dt} = \frac{\hat{F}_{i-1/2,j,k} - \hat{F}_{i+1/2,j,k}}{\Delta x} + \frac{\hat{G}_{i,j-1/2,k} - \hat{G}_{i,j+1/2,k}}{\Delta y} + \frac{\hat{H}_{i,j,k-1/2} - \hat{K}_{i,j,k+1/2}}{\Delta z} + S_{i,j,k} \tag{16}$$

where $U_{i,j,k}$ is an approximation to the point value $U(x_i, y_j, z_k, t)$ of the solution. The numerical fluxes $\hat{F}_{i\pm1/2,j,k}$, $\hat{G}_{i,j\pm1/2,k}$ and $\hat{H}_{i,j,k\pm1/2}$ can be computed using the known grid values of $F_{i,j,k}$, $G_{i,j,k}$ and $H_{i,j,k}$ by a WENO reconstruction. The classical ($2r$-1)-th order WENO scheme uses a ($2r$-1)-point stencil to approximate the numerical flux, which is divided into r substencils $S_0, S_1, \ldots, S_{r-1}$ with each substencil containing r grid points.

Take $\hat{F}_{i+1/2,j,k}$ as an example. The WENO reconstruction is made as follows. We first perform a Lax-Friedrichs flux splitting for the flux $F_{i,j,k}$ on the node, obtaining

$$F^+_{i,j,k} = \frac{1}{2}\left(F(U_{i,j,k}) + \alpha U_{i,j,k}\right), \qquad F^-_{i,j,k} = \frac{1}{2}\left(F(U_{i,j,k}) - \alpha U_{i,j,k}\right) \tag{17}$$

where $\alpha = \max_{1\le i\le n_x} |\lambda(U_{i,j,k})|$, for fixed j and k, with $\lambda(U_{i,j,k})$ being the largest (in absolute value) eigenvalue of the Jacobian $A(U) = \frac{\partial F}{\partial U}$. It is also possible to take the maximum locally and/or to take the maximum over individual eigenvalues, to reduce numerical dissipation, see [2] for more details. We then construct also two numerical fluxes $\hat{F}^+_{i+1/2,j,k}$ and $\hat{F}^-_{i+1/2,j,k}$, approximating F^+ and F^- respectively, and their sum will be the numerical flux $\hat{F}_{i+1/2,j,k}$. Below we will give the details of the construction of the numerical flux $\hat{F}^+_{i+1/2,j,k}$ only, as the procedure to construct the numerical flux $F^-_{i,j,k}$ is symmetric to that for $F^+_{i,j,k}$ with respect to the location $i + 1/2$. The ($2r$-1)-th order numerical flux $\hat{F}^+_{i+1/2,j,k}$ is built through a convex combination of the r-th order numerical fluxes $\hat{F}^{+,(l)}_{i+1/2,j,k}$ based on the substencils

$$\hat{F}^+_{i+1/2,j,k} = \sum_{l=0}^{r-1} \omega_l \hat{F}^{+,(l)}_{i+1/2,j,k} \tag{18}$$

where ω_l are the nonlinear weights, satisfying $\omega_l \ge 0$ and $\sum_{l=0}^{r-1} \omega_l = 1$. If no discontinuity exists on the large stencil, there are positive linear weights d_l which yield

$$\hat{F}^+_{i+1/2,j,k} = \sum_{l=0}^{r-1} d_l \hat{F}^{+,(l)}_{i+1/2,j,k} = \hat{F}(x_{i+1/2}, y_j, z_k) + O(\Delta x^{2r-1}) \tag{19}$$

where $\hat{F}(x_{i+1/2}, y_j, z_k)$ is the theoretically infinite order accurate flux. We again refer to [2] for more details.

By consistency $\sum_{l=0}^{r-1} d_l = 1$. In smooth regions, we would require $\omega_l = d_l + O(\Delta x^{r-1})$. In WENO schemes, the nonlinear weight function should be smooth. Moreover, when the substencil contains discontinuities, the corresponding weight ω_l should be very small. The weights in [2] are defined as

$$\omega_l = \frac{\alpha_l}{\sum_{s=0}^{r-1} \alpha_s}, \qquad l = 0, \ldots, r-1; \qquad \alpha_l = \frac{d_l}{(\varepsilon + \beta_l)^2}. \tag{20}$$

The smoothness indicators β_l are given by

$$\beta_l = \sum_{n=1}^{r-1} \Delta x^{2n-1} \int_{x_{i-1/2}}^{x_{i+1/2}} \left(\frac{d^n \hat{F}^{\pm(l)}(x,y,z)}{dx^n} \right)^2 dx \tag{21}$$

where $\hat{F}^{\pm(l)}(x,y,z)$ is the reconstruction polynomial for the l-th substencil, the parameter ε is used to avoid the division by zero in the denominator, and is taken as 10^{-6} in the

simulation. In the case of $r = 3$, the resulting WENO scheme is fifth-order accurate, with a 5-point big stencil S^5, and three substencils S_0, S_1, S_2, each containing 3-points. For the substencil S_0 one has

$$\hat{F}^{+,(0)}_{i+1/2,j,k} = \frac{1}{3}F^+_{i-2,j,k} - \frac{7}{6}F^+_{i-1,j,k} + \frac{11}{6}F^+_{i,j,k} \tag{22}$$

for the substencil S_1 one has

$$\hat{F}^{+,(1)}_{i+1/2,j,k} = -\frac{1}{6}F^+_{i-1,j,k} - \frac{5}{6}F^+_{i,j,k} + \frac{1}{3}F^+_{i+1,j,k} \tag{23}$$

and for the substencil S_2 one has

$$\hat{F}^{+,(2)}_{i+1/2,j,k} = \frac{1}{3}F^+_{i,j,k} + \frac{5}{6}F^+_{i+1,j,k} - \frac{1}{6}F^+_{i+2,j,k} \tag{24}$$

The linear weights are $d_0 = 3/10$, $d_1 = 3/5$ and $d_2 = 1/10$. The three smoothness indicators are:

$$\beta_0 = \frac{13}{12}(F^+_{i-2,j,k} - 2F^+_{i-1,j,k} + F^+_{i,j,k})^2 + \frac{1}{4}(F^+_{i-2,j,k} - 4F^+_{i-1,j,k} + 3F^+_{i,j,k})^2 \tag{25}$$

$$\beta_1 = \frac{13}{12}(F^+_{i-1,j,k} - 2F^+_{i,j,k} + F^+_{i+1,j,k})^2 + \frac{1}{4}(F^+_{i-1,j,k} + F^+_{i+1,j,k})^2 \tag{26}$$

$$\beta_2 = \frac{13}{12}(F^+_{i,j,k} - 2F^+_{i+1,j,k} + F^+_{i+2,j,k})^2 + \frac{1}{4}(3F^+_{i,j,k} - 4F^+_{i+1,j,k} + F^+_{i+2,j,k})^2. \tag{27}$$

Using the same procedure, the numerical fluxes in y and z directions $\hat{G}^{\pm}_{i,j+1/2,k}$ and $\hat{H}^{\pm}_{i,j,k+1/2}$ can also be constructed. We take

$$\hat{F}_{i+1/2,j,k} = \hat{F}^+_{i+1/2,j,k} + \hat{F}^-_{i+1/2,j,k} \tag{28}$$

$$\hat{G}_{i,j+1/2,k} = \hat{G}^+_{i,j+1/2,k} + \hat{G}^-_{i,j+1/2,k} \tag{29}$$

$$\hat{H}_{i,j,k+1/2} = \hat{H}^+_{i,j,k+1/2} + \hat{H}^-_{i,j,k+1/2} \tag{30}$$

Then the numerical scheme (16) is formed. If we denote its right hand side as $L(U_{i,j,k})$, then the fully discrete scheme, using the third-order TVD Runge-Kutta scheme [42] for temporal discretization, is given as

$$\begin{cases} U^{(1)}_{i,j,k} = U^n_{i,j,k} + \Delta t L(U^n_{i,j,k}) \\ U^{(2)}_{i,j,k} = \frac{3}{4}U^n_{i,j,k} + \frac{1}{4}U^{(1)}_{i,j,k} + \Delta t L(U^{(1)}_{i,j,k}) \\ U^{n+1}_{i,j,k} = \frac{1}{3}U^n_{i,j,k} + \frac{2}{3}U^{(2)}_{i,j,k} + \Delta t L(U^{(2)}_{i,j,k}) \end{cases}$$

When studying three-dimensional detonation problems, due to the very large size of the computational domain and a large number of grid points, it is essential to implement the WENO scheme in an efficient three-dimensional parallel code to be used on a massively parallel platform, which is carried out in this paper.

4 Results and discussion

4.1 Grid convergence study on a one-dimensional mildly unstable detonation

For this study we take the parameters as $f = 1.6$, $Ea = 50.0$, $Q = 50.0$, and $K = 230.75$[43]. The size of the computational domain is $1000 \times L_{1/2}$, where $L_{1/2}$ is the length of a half reaction zone. The one-dimensional ZND analytical solution is used as the initial condition. The left boundary is an inflow, and the right boundary is an outflow. Three resolutions employed in the simulations are $5pts/L_{1/2}$ (i.e. 5 points in the length of a half reaction zone), $10pts/L_{1/2}$ and $20pts/L_{1/2}$, respectively. The final time is $t = 100$. For a one-dimensional unstable detonation, the round-off error is enough to provide an initial perturbation, which further triggers the physical instability of the detonation. Therefore, it is unnecessary to artificially add any initial perturbation. Figure 1 illustrates the ZND front pressure time histories for the three grid resolutions. It can be seen from Figure 1 (a) that, when the grids become finer, the front pressure peak-time curve tends to be consistent, and the pressure curves corresponding to $10pts/L_{1/2}$ and $20pts/L_{1/2}$ are largely overlapping, indicating the numerical computation is convergent. Furthermore, the advantages of the fifth order WENO scheme can be found, i.e., the ZND pressure peak for $10pts/L_{1/2}$ is 98.58; for $20pts/L_{1/2}$ it is 98.6, which is in close agreement with the theoretical value $P_{max} = 98.6$ [44]. Comparing the curves in Figure 1 (b) it can be seen that, for the one-dimensional mildly unstable detonation, to reach the theoretical value 98.6, it is enough for the fifth order WENO scheme to use only $10pts/L_{1/2}$. The number of grids used is obviously decreased compared with other algorithms, e.g. [45]. Moreover, with an increasing grid point number the desired resolution is quickly obtained.

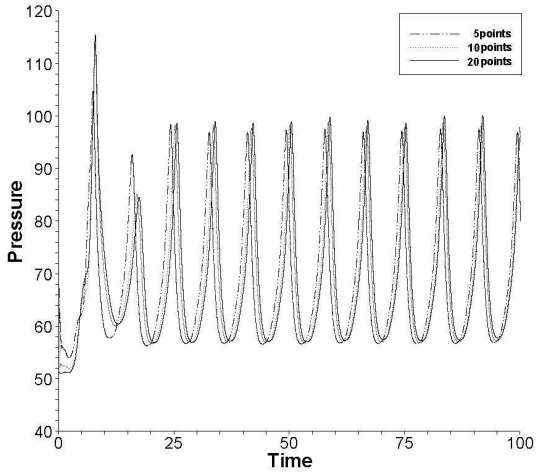

a)

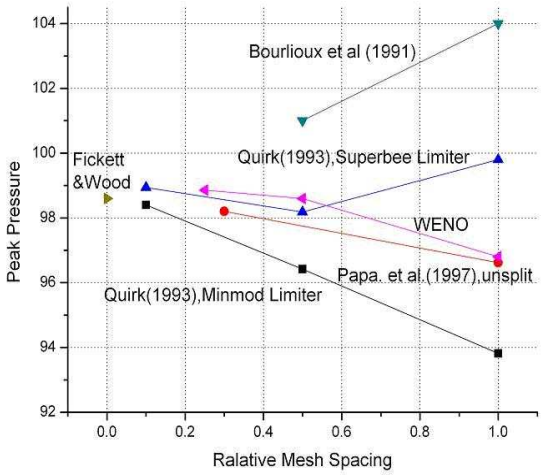

b)

Figure 1: Grid convergence study with the mildly unstable detonation (overdrive factor $f = 1.6$). The theoretically predicted value is $P_{max} = 98.6$.

4.2 Study on two-dimensional detonations

The propagation mode and cellular structure of two-dimensional unstable detonations with different overdrive factors and different computational domain widths are studied to provide reference to the simulation of three-dimensional detonation structures. We adopt the one-dimensional ZND analytical solution as the initial condition, and add a very small transverse perturbation to the ZND profile. The left boundary is an inflow boundary, and the right boundary is an outflow boundary. The upper and bottom boundaries are solid walls.

4.2.1 Influence of different overdrive factors on two-dimensional detonation cell widths

In order to study the detonation cellular width with high activation energy at different overdrive factors, the computational domain is set as $[240,\ 4]\times L_{1/2}$. The chemical reaction parameters are listed in Table 1. Figure 2 shows the maximum pressure history of the detonation at different overdrive factors. Due to the very small width-length ratio of the duct, the complete computational domain is divided into three sections for showing the maximum pressure history. It can be seen from the figure that, with a decreasing overdrive factor, the cell width reduces. When $f = 1.0$, the cell width is about $3\times L_{1/2}$, the width-length ratio of the cell is 0.50. When $f = 1.2$ and $f = 1.6$, no complete cell can be formed because the transverse wavelength is larger than the duct width. Thus it can be seen that, with an increasing overdrive factor, the transverse wavelength increases.

Table 1: Overdrive factor and pre-exponential factor ($Ea = 50.0$, $Q = 50.0$)[20, 43]

	A	B	C
Overdrive factor f	1.0	1.2	1.6
Pre-exponential factor K	2566.42	871.42	230.75

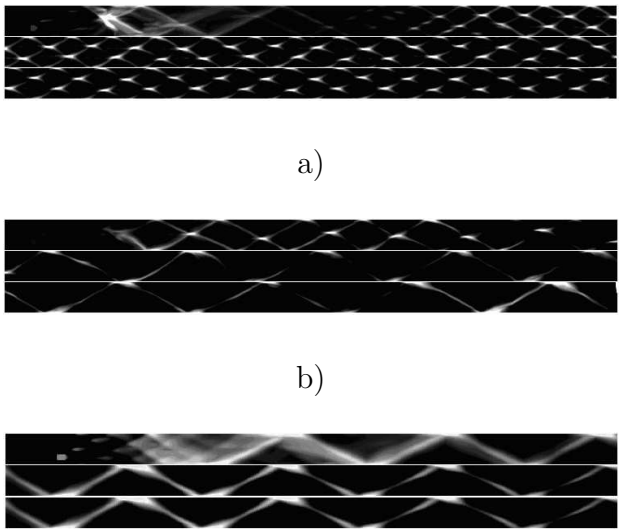

a)

b)

c)

Figure 2: Maximum pressure history of detonation at different overdrive factors. a) $f = 1.0$, b) $f = 1.2$, c) $f = 1.6$.

4.2.2 Influence of the two-dimensional computational domain width on unstable detonation propagation

One-dimensional linear stability analysis suggests that, the detonation stability is, to a large extent, dependent on the selected reaction parameters. Lee and Stewart [43] pointed out that, at given f, Q and γ, with an increasing activation energy, the detonation becomes unstable. In this section, the influence of the duct width on the detonation propagation mode is numerically investigated. In the computation, we take $Ea = 50.0$, $Q = 50.0$, and $f = 1.0$ as the parameters. The duct width is taken as $1\times L_{1/2}$, $2\times L_{1/2}$, $4\times L_{1/2}$, $8\times L_{1/2}$ and $16\times L_{1/2}$ respectively, and the duct length is $240\times L_{1/2}$. Figure 3 displays the maximum pressure history for the computational domain of different widths. When the width is $1\times L_{1/2}$ and $2\times L_{1/2}$, no complete detonation cells can be formed. When the width is $8\times L_{1/2}$ and $16\times L_{1/2}$, detonation cells can be formed, but they are uneven. Average width-length ratio of the cells measured is about 0.51, which is slightly smaller than 0.55 that was measured in [12].

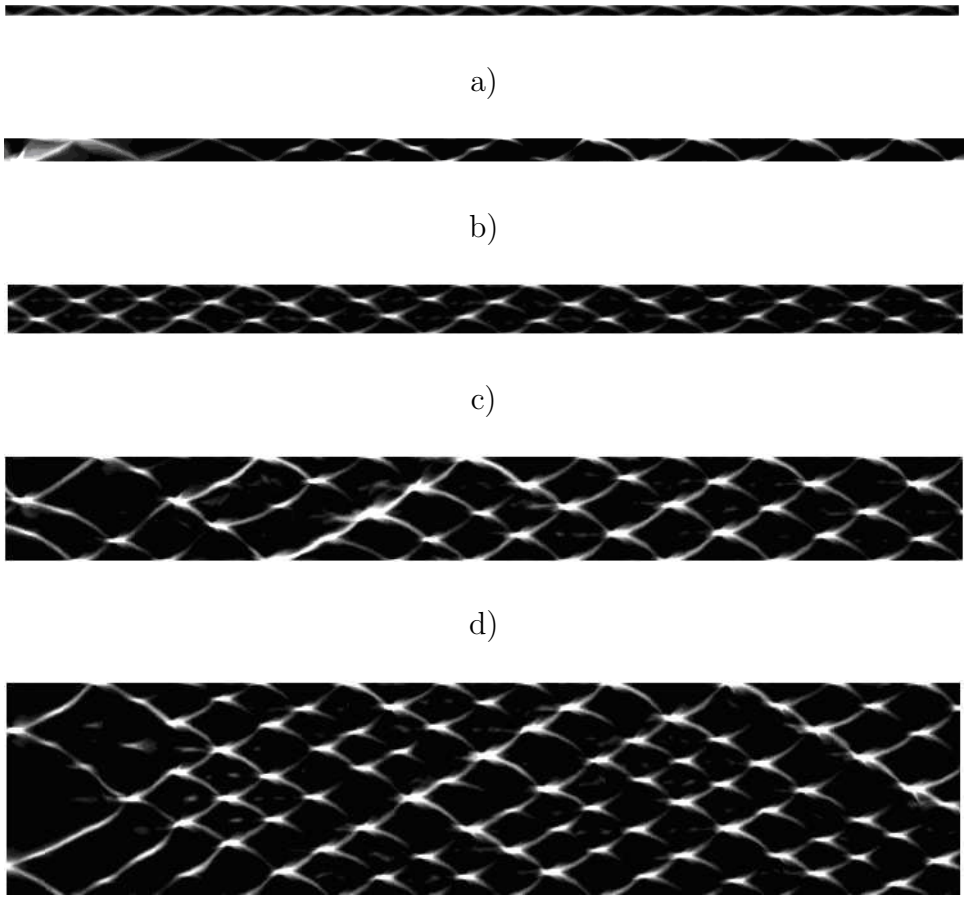

Figure 3: Maximum pressure history: a) $1\times L_{1/2}$, b) $2\times L_{1/2}$, c) $4\times L_{1/2}$, d) $8\times L_{1/2}$, e) $16\times L_{1/2}$.

4.3 Study on three-dimensional detonations

We use the one-dimensional ZND analytical solution as the initial condition, and add a very small perturbation in the ZND profile to accelerate the unstable growth of the flow. Unless otherwise indicated, the left boundary of the duct is an inflow, the right boundary is an outflow, and the remaining sides are rigid walls. The detonations propagate along the x-direction. Simulations of three-dimensional detonations demand high grid resolution, especially for unstable detonations. Therefore, a grid resolution of $20pts/L_{1/2}$ is employed to cover the computational domain.

4.3.1 Verification of the numerical resolution of three-dimensional detonations

We add source terms (functions of x, y, z and t) to the PDE system so that the following functions are exact solutions to the modified PDE system:

$$\rho(x, y, z, t) = 1 + \tfrac{1}{2}\sin(\pi(x + y + z - 2t))$$

$$u(x, y, z, t) = v(x, y, z, t) = w(x, y, z, t) = p(x, y, z, t) = 1$$

$$Y(x, y, z, t) = \tfrac{1}{2} + \tfrac{1}{2}\sin(\pi(x - 2y + 2z + t)) \ .$$

The initial condition is set to be

$$\rho(x, y, z, t) = 1 + \tfrac{1}{2}\sin(\pi(x + y + z))$$

$$u(x, y, z, 0) = v(x, y, z, 0) = w(x, y, z, 0) = p(x, y, z, 0) = 1$$

$$Y(x, y, z, 0) = \tfrac{1}{2} + \tfrac{1}{2}\sin(\pi(x - 2y + 2z)) \ .$$

The parameter values $Ea = 50.0$, $f = 1.6$, and $Q = 50.0$ are given, and the computational domain is taken as $[0,\ 2]\times[0,\ 2] \times [0,\ 2]$. We use uniform meshes with periodic boundary conditions, and give the errors and orders of accuracy for the density at time $t = 2.0$ in Table 2. It can be observed clearly that the designed fifth order accuracy is achieved.

Table 2: L^∞, L^1 and L^2 errors and orders of accuracy for the density

h	CFL	L^∞Error	Order	L^1Error	Order	L^2Error	Order
2/20	0.2	1.26×10^{-3}		8.13×10^{-4}		8.96×10^{-3}	
2/40	0.2	4.48×10^{-5}	4.84	2.46×10^{-5}	4.93	2.74×10^{-5}	5.05
2/80	0.2	1.32×10^{-6}	5.23	7.50×10^{-7}	5.05	8.12×10^{-7}	5.09
2/160	0.2	4.35×10^{-8}	4.95	2.15×10^{-8}	5.14	2.44×10^{-8}	5.08
2/320	0.2	1.16×10^{-9}	5.25	6.92×10^{-10}	4.98	9.01×10^{-10}	4.78

4.3.2 Influence of the duct width on three-dimensional detonations

From the numerical results for two-dimensional detonations, we have seen that, when $f = 1.0$, $Q = 50.0$, and $Ea = 50.0$, the transverse wavelength of the unstable detonation is very small, and the cellular width is relatively small. It is appropriate to choose this set of chemical reaction parameters to study the influence of three-dimensional duct width on detonation propagation modes. We study three-dimensional square ducts, with length $160\times L_{1/2}$, and with width $1\times L_{1/2}$ (Case 1), $2\times L_{1/2}$ (Case 2), $4\times L_{1/2}$ (Case 3), $8\times L_{1/2}$ (Case 4) and $16\times L_{1/2}$ (Case 5), respectively. From our experience in the grid convergence study on one-dimensional unstable detonation, we can see that $10pts/L_{1/2}$ can meet the required computational accuracy. However, for three-dimensional unstable detonations, more number of grid points is required for the half reaction zone [46, 6, 47]. Hence, $20pts/L_{1/2}$ is adopted in our computation. We use the one-dimensional ZND analytical solution as the initial condition, and add a very small transverse sinusoidal perturbation to the ZND profile. Parallel computation is performed by using high-performance computers. The computational domain, number of grid points and number of MPI processors are shown in Table 3.

Table 3: Computational domain, number of grid points and number of MPI processors

Case	1	2	3	4	5
Domain	$[160,1,1]\times L_{1/2}$	$[160,2,2]\times L_{1/2}$	$[160,4,4]\times L_{1/2}$	$[160,8,8]\times L_{1/2}$	$[160,16,16]\times L_{1/2}$
Grids	$3200\times20\times20$	$3200\times40\times40$	$3200\times80\times80$	$3200\times160\times160$	$3200\times320\times320$
Processors	64	180	270	360	450

Figure 4 shows, in the duct with width $2\times L_{1/2}$, the typical front feature and density

gradient on the walls of the detonation in a cycle. The front structure is similar to that in [48, 49], suggesting spinning detonations have formed. Due to the differences in the type of perturbation, spinning detonation rotates counter-clockwise, opposite to that in [48]. It can be seen that, the triple lines and transverse waves collide with the walls, and strong explosions take place near the walls. Transverse waves play an important role in changing the spinning direction.

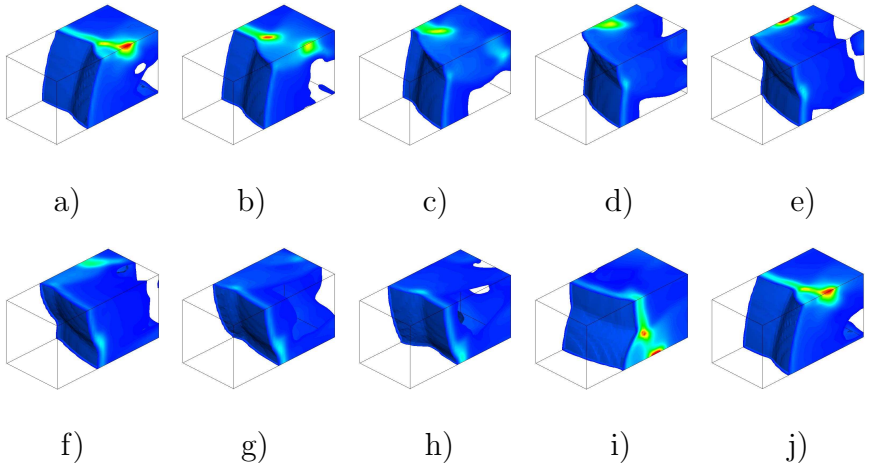

Figure 4: Typical spinning detonation density contour of the detonation front for a full cycle. Frames(a)-(j) are equally spaced with the same time.

Figure 5 (a, b, c) displays the maximum pressure history and the main spinning tracks on the walls when the detonations for Case 1, Case 2 and Case 3 appear spinning mode. It can be clearly seen from these pictures that the spinning tracks of the single-headed detonations on the walls propagate counter-clockwise along the walls. For Case 1, the main spinning dominates. Because transverse waves are restricted by the walls, they are not completely developed. Colliding with the duct corner, the triple lines are not strongly reflected. Hence, the tracks of the reflected triple lines are not apparent. After the stable single-headed spinning detonation is formed for a time period, its pressure decreases, and ultimately it cannot stably propagate. With width increasing,the spinning detonation formed can stably propagate and the tracks of the reflected triple points become more obvious, as shown in Figure 5(c). Figure 6 shows the maximum pressure history on the unfolded walls for Case

1, Case 2 and Case 3. It can be seen from this figure that, for Case 2 and Case 3, a stable single-headed spinning detonation is formed. The main spiral and the tracks of reflective triple point characterized by single-headed spinning detonations [36, 27] are shown on the rigid walls. Comparing the computational results for Case 2 and Case 3, we can see that, when the width is doubled, the cycle of the spinning detonation also doubles. [50, 51] gave the theoretical value of the pitch-to-diameter ratio of the spinning detonation in a round duct as

$$\frac{p_1}{d} = \frac{\pi(\gamma+1)}{1.841\gamma}$$

where p_1 is the pitch of spin, and d is the duct diameter. The above formula indicates that the pitch-to-diameter ratio is related only to the specific heat of gas. For the gas having γ=1.2, the pitch-to-diameter ratio is 3.128. Although the theoretical value was obtained in the round duct, it should be applicable also to a rectangular duct. Through the maximum pressure history on the walls, we can measure the pitch-to-diameter ratio of Case 3 as 3.42, which is slightly larger than the theoretical value, and also larger than 2.7, the pitch-to-diameter ratio measured in [26]. The measured spinning angle, which can be computed by the length covered by the detonation front along the x-direction in a cycle and the duct perimeter, is 51.5° for Case 2, and is 49.5° for Case 3. They are in good agreement with the results in [49, 52]. Therefore, width change exerts little influence on the spinning angle. When the width increases to the one for Case 4, irregular cells are shown on the walls, as shown in Figure 7. When the width is further increased to Case 5, transverse perturbations are little affected by the width. Over time, obvious out-of-phase slapping waves are displayed on the walls. Detonation gradually evolves into an out-of-phase rectangular mode,as shown in Figure 8. The feature coincides with that in [24]. The measured cellular width is about $4.5\times L_{1/2}$, larger than that in the two-dimensional computational results shown in Figure 3 (c). It seems that $4.5\times L_{1/2}$ is the critical width for the formation of spinning detonations. When the duct width is smaller than this value, spinning detonations can be triggered. For wider ducts, the wall boundary conditions exert little influence on the transverse waves,

so the measured cell width can be believed as the true width of the unstable detonation. Comparing the computational results for Cases 1-5, we can conclude that, when the duct width is smaller than the cell width, the unstable detonation propagates in a spinning mode; when the duct width is larger than the cell width, spinning detonation disappears.

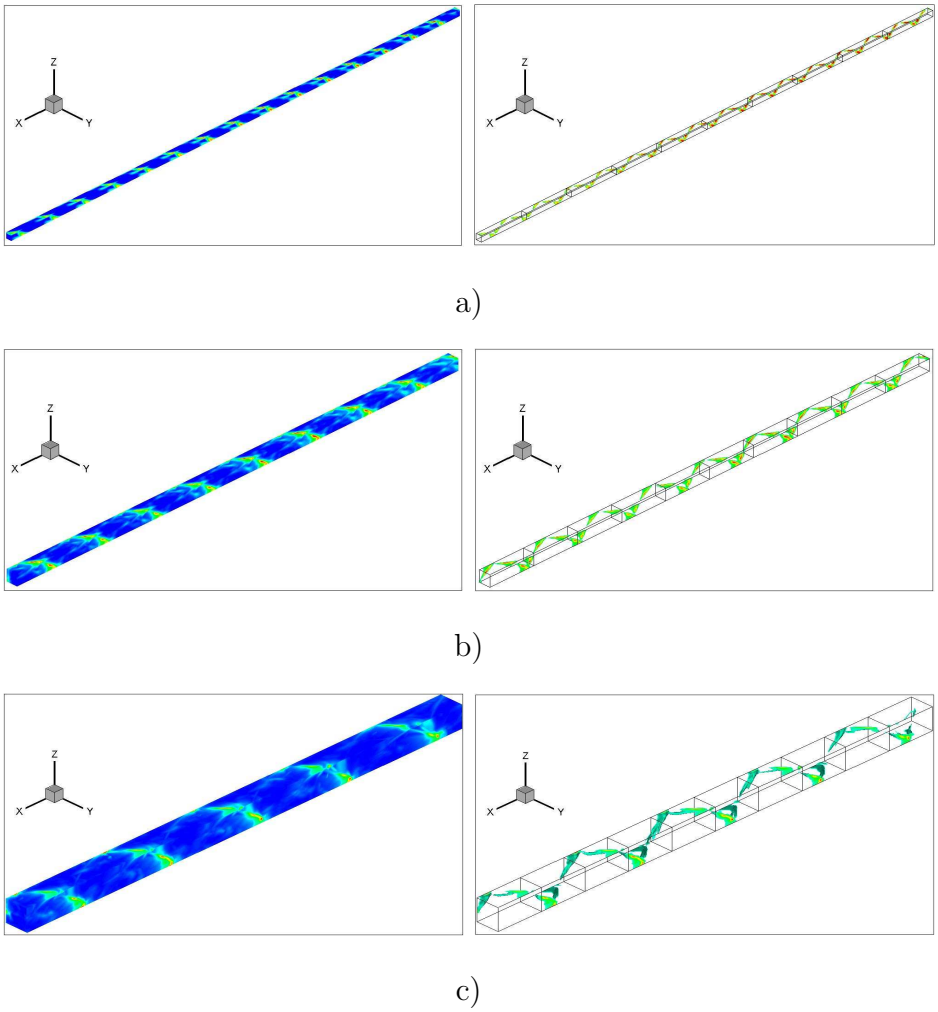

Figure 5: Maximum pressure history and main spinning tracks on the walls (Detonation wave propagates along the x-direction): a) Case 1, b) Case 2, c) Case 3.

In order to study the influence of the overdrive factor on the spinning detonation, we take $f = 1.2$, $Q = 50.0$ and $Ea = 50.0$. The duct width is the same as the one for Case 2. Figure 9 shows the maximum pressure history of the highly unstable detonation on the duct walls. Comparing Figure 6 (b) with Figure 9, we can see that the two unstable detonations

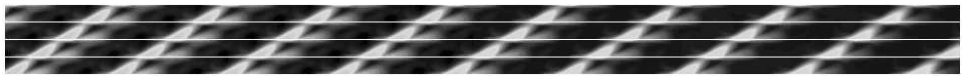

a)

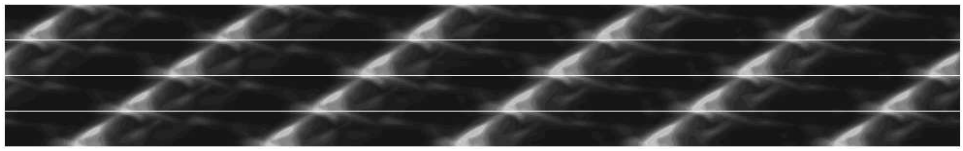

b)

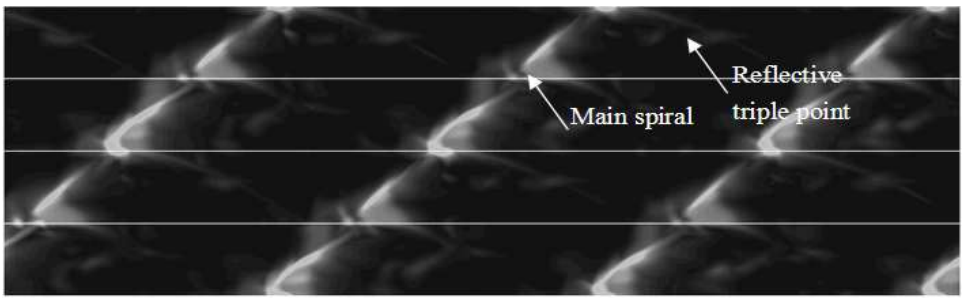

c)

Figure 6: Maximum pressure history of the spinning detonation on the walls: a) Case 1, b) Case 2, c) Case 3 (detonation wave propagates from left to right).

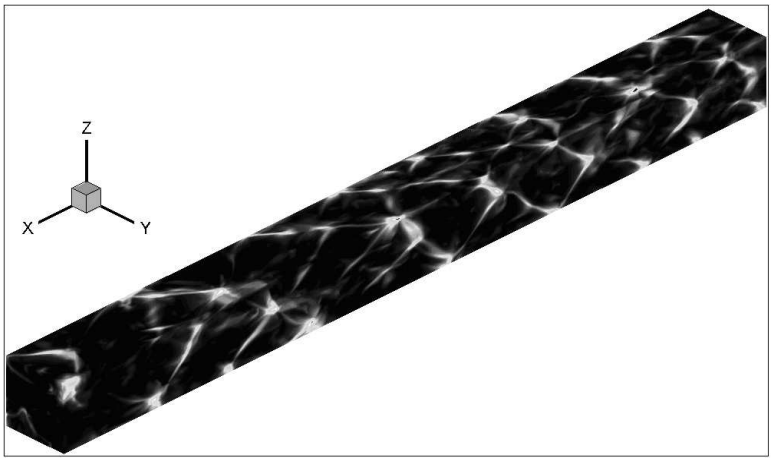

Figure 7: Maximum pressure history on the walls: Case 4.

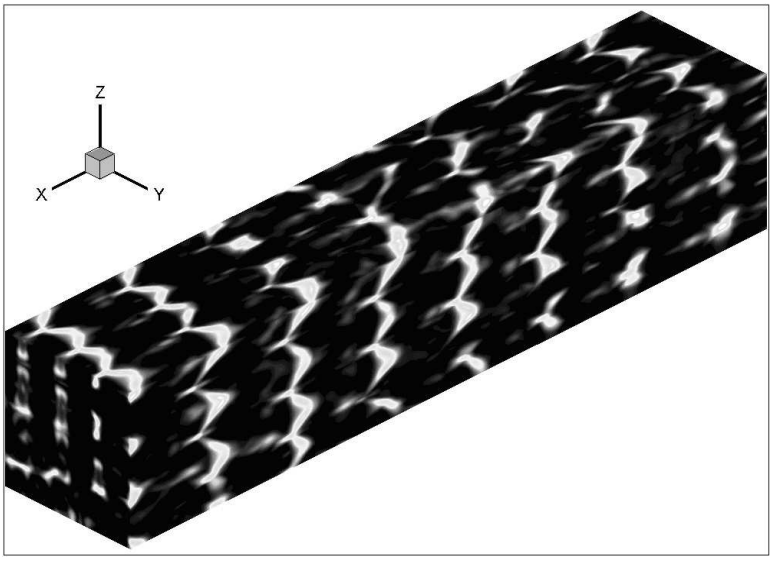

Figure 8: Maximum pressure history on the walls: Case 5.

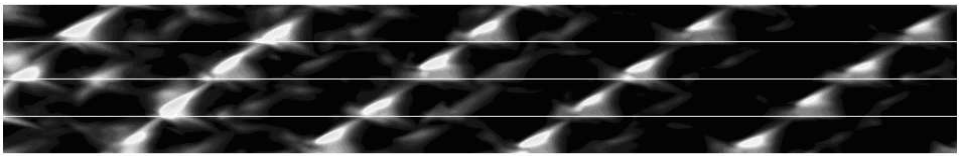

Figure 9: Maximum pressure history of the spinning detonation on the walls: $f = 1.2$, $Q = 50.0$, $Ea = 50.0$ (detonation wave propagates from left to right).

can trigger the spinning mode in the duct with width $2\times L_{1/2}$, and the measured spinning angle and pitch-to-diameter ratio in the two cases are equal. This is because the transverse wavelength at $f = 1.2$ is larger than that at $f = 1.0$, which has been obtained from the two-dimensional computational results,as shown in Figure 2.

4.3.3 Detonation structure at different chemical reaction parameters under different types of perturbation

With different chemical reaction parameters, the three-dimensional detonation front features and propagation mode under transverse cosine and symmetrical perturbation along the diagonal direction is investigated. Give three groups of chemical reaction parameters: (1) $Ea = 20.0,\ Q = 2.0,\ f = 1.1$ and $K = 1134363.64$, corresponding to the one-dimensional problem which is a stable detonation [43]; (2) $Ea = 50.0,\ Q = 50.0,\ f = 1.6$ and $K = 230.75$, corresponding to the one-dimensional problem which is a mildly unstable detonation [53]; (3) $Ea = 50.0,\ Q = 50.0,\ f = 1.2$ and $K = 871.42$, which corresponds to a case with high activation energy and high heat of reaction, and, according to a linear stability analysis in Erpenbenk [53] and Lee and Stewart [43], the corresponding one-dimensional problem is unstable. Erpenbenk [54] also proposed that the corresponding two-dimensional problem is a highly unstable detonation for this case (3).

The initial condition is the one-dimensional ZND analytical solution, and transverse cosine perturbation or symmetrical perturbation along the diagonal direction is added to the ZND profile. We take the computational domain in length, width and height as [144, 9.6, 9.6]$\times L_{1/2}$. A grid with 2880×192×192 points are used.

(1) The detonation structure under transverse cosine perturbation

- Stable detonation ($Ea = 20.0,\ Q = 2.0,\ f = 1.1$)

We take $5pts/L_{1/2}$, $10pts/L_{1/2}$ and $20pts/L_{1/2}$ to verify the grid resolution and the convergence of the numerical method. Figure 10 gives the pressure gradient distribution at $t = 60.0$ on the wall ($y = 0$). It can be seen that, the finer the grid, the clearer the front structure.

At $5pts/L_{1/2}$, the global features of the flow can be seen only roughly. At $10pts/L_{1/2}$, the detonation front structure and the flow features have been reasonably well captured, however the image resolution is not high. At $20pts/L_{1/2}$, the detonation front structure and flow features are captured very well.

Figure 11 records the maximum pressure history on the walls. It can be seen from this figure that the triple-line trajectories form regular cellular structures. Detonation cells are regular. The width-length ratio of the cell is measured to be 0.51, which is close to the two-dimensional result measured in [12, 13]. The slapping waves orthogonal to each other are displayed on the walls. The slapping waves are parallel to the y and z-directions, respectively, which is in agreement with the result in [24]. Figure 12 displays the front structure and the pressure gradient on the walls. It can be seen in this figure that the detonation wave has a rectangular structure, and the front contains four pairs of triple lines, two of which are parallel to the y-direction and the other two parallel to the z-direction. When each pair of the triple lines moves in opposite directions parallel to the front, a pair of triple lines will collide with the walls or with each other. When the triple line collides with the walls, slapping waves are shown on the walls. But when a pair of triple lines collide with each other, the triple line parallel to the propagation direction will appear. Because the perturbation mode is in phase, the triple lines parallel to the y-direction and to the z-direction arrive at the walls at the same time, and they collide with the walls. In-phase slapping waves appear on the walls. Hence, under transverse cosine perturbation, detonation waves propagate in in-phase rectangular mode. Figure 13 displays the density gradient and front structure on the walls. From this figure, the triple line movement direction and their collision with the walls can be observed more clearly.

- Mildly unstable detonation ($Ea = 50.0,\ Q = 50.0,\ f = 1.6$)

We take $5pts/L_{1/2}$, $10pts/L_{1/2}$ and $20pts/L_{1/2}$ to verify the grid resolution and convergence of the mildly unstable detonation under transverse cosine perturbation. Figure 14 gives the pressure gradient distribution on the wall ($y = 0$) at $t = 40.0$. It can be seen that

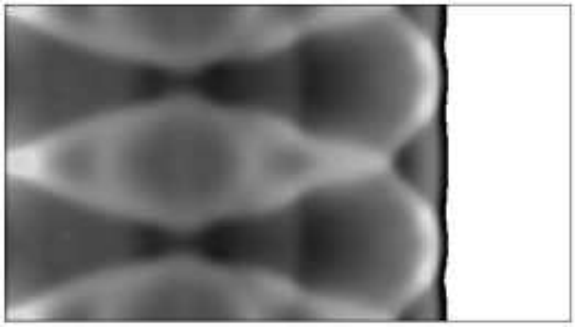

a)

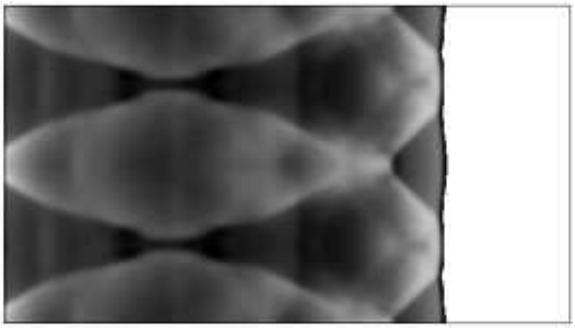

b)

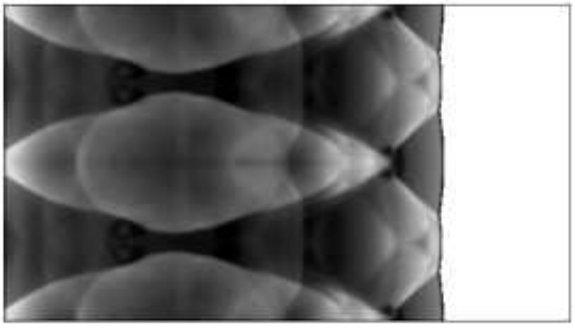

c)

Figure 10: Grid resolution: a) $5pts/L_{1/2}$, b) $10pts/L_{1/2}$, c) $20pts/L_{1/2}$.

Figure 11: Maximum pressure history on the walls.

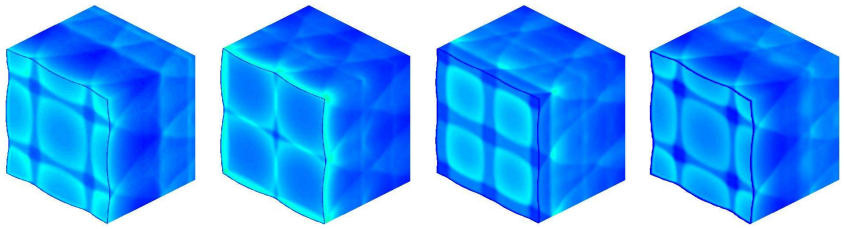

a)t=21.5 b)t=23.5 c)t=25.5 d)t=27.5

Figure 12: Front structure and pressure gradient on the walls.

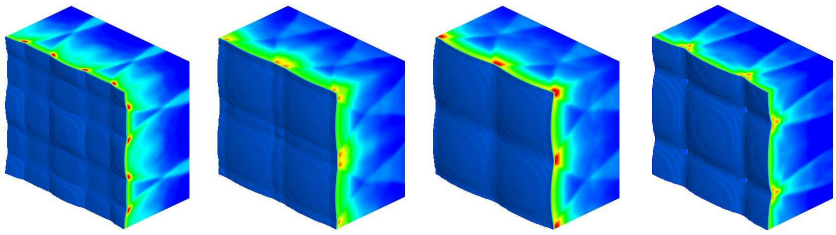

a)t=20.5 b)t=22.5 c)t=23.5 d)t=25.5

Figure 13: Rectangular front structure and density gradient on the walls.

at $20pts/L_{1/2}$, the detonation front structure and flow features can be captured very well.

Figure 15 displays the evolution of a mildly unstable detonation front and the density gradient on the walls. At $t = 1.46$, due to flow instability, local overdrive is obvious, leading to a highly distorted detonation front. At $t = 6.87 - 10.62$, detonations enter into a low velocity stage, the particles penetrating into the front need a very long induction period. The front becomes flat, the front thickness increases, and combustion is incomplete. Over time, detonations re-appear. Due to the nature of such detonation instability, the triple lines are relatively bent, and the front shows "convex" and "concave" features. At $t = 13.29$, the front is relatively distorted, but still maintains a rectangular structure. The triple lines on the front, parallel to the x- or the y-directions, move toward the walls, and collide with the walls and then are reflected, moving at opposite directions. At $t = 23.49$, they collide once again on the central line. For three-dimensional detonations, the concave part on the front is equivalent to the Mach stem in the two-dimensional case. The flow between the concave part and other concave parts is incident waves. At $t = 32.11 - 33.48$, the triple lines collide with the walls. Local explosions occur at the wall corner, and the front is very distorted, leading to inconsistent reaction rate behind the front. Hence, a large quantity of unreacted pockets appear behind the front (Figure 16 (a,b)). It can be seen from Figure 16 (b) that in-phase slapping waves appear on the walls, and become thick and bent. This is because of the flow instability and high overdrive leading to an increase of unreacted substances. The measured width-length ratio of the cells is 0.46, which is consistent with the result in [24].

• Highly unstable detonation ($Ea = 50.0,\ Q = 50.0,\ f = 1.2$)

For three-dimensional highly unstable detonations, the precursor shock peak can reach 1.5 times the stable ZND peak, and the length of the reaction zone significantly decreases [51]. Therefore, higher grid resolution is needed. We take $5pts/L_{1/2}$, $10pts/L_{1/2}$ and $20pts/L_{1/2}$ to verify grid resolution and convergence of the numerical method. Figure 17 gives the pressure gradient distribution of such detonations at $t = 10.0$ on the walls ($y = 0$). It can be seen that, as the grids are refined, the numerical results show good convergence, and the front

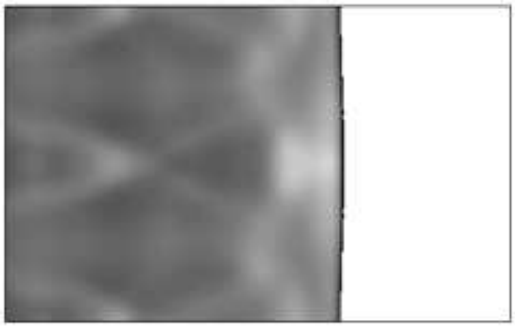

a)

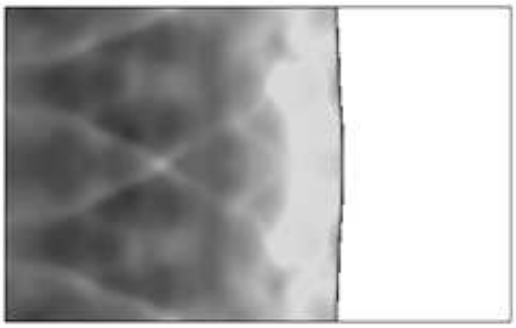

b)

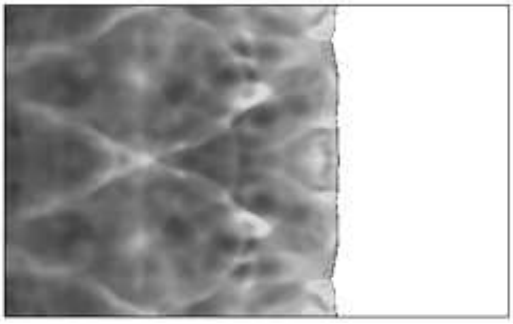

c)

Figure 14: Grid resolution: a) $5pts/L_{1/2}$, b) $10pts/L_{1/2}$, c) $20pts/L_{1/2}$.

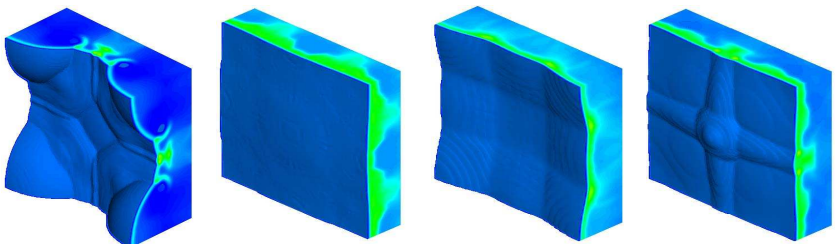

a)$t = 1.46$ b)$t = 6.87$ c)$t = 8.75$ d)$t = 10.62$

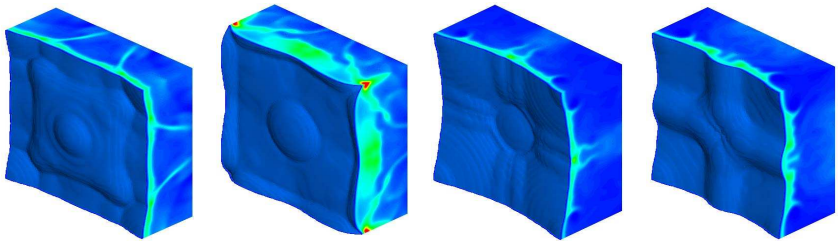

e)$t = 13.29$ f)$t = 18.84$ g)$t = 23.49$ h)$t = 23.86$

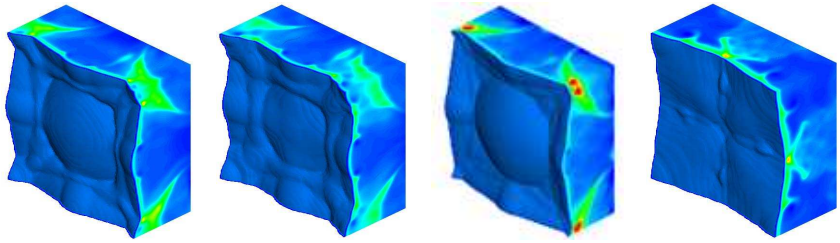

i)$t = 32.11$ j)$t = 32.56$ k)$t = 33.02$ l)$t = 33.48$

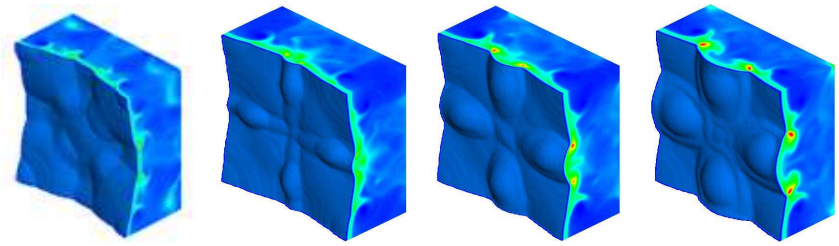

m)$t = 34.06$ n)$t = 34.42$ o)$t = 34.84$ p)$t = 35.22$

Figure 15: Front structure and density gradient on the walls at different times.

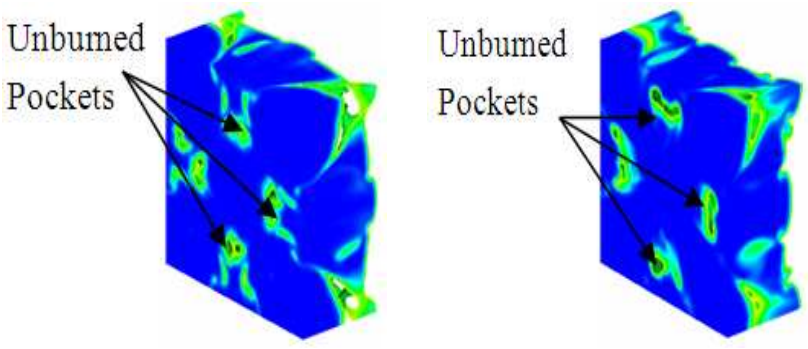

a) b)

Figure 16: Unreacted pockets behind the detonation front.

structure becomes clearer. At $5pts/L_{1/2}$, the grids are too coarse to resolve global features of the flow for this case. At $10pts/L_{1/2}$, the global flow features of the detonations can be roughly captured, but the meso features of the front cannot be clearly captured. At $20pts/L_{1/2}$, the front structure and flow features of detonations can be captured very well. It seems that, for highly unstable detonations, $20pts/L_{1/2}$ can describe the front structure well by our numerical method.

Figure 18 gives the front structure of the highly unstable detonation and the density gradient at different times. It can be seen that the detonation front has a rectangular structure at the early stage. At $t = 10.71$, the front becomes flat and thick, and the detonation velocity decreases. After a low velocity stage for a long period of time, at $t = 24.93 - 28.43$, detonations reappear, at which time the front still has a rectangular structure. Highly unstable flow leads to a big local overdrive, distorted front and asymmetrical triple lines. At $t = 39.30 - 42.61$, many triple lines appear on the front, and the front structure becomes complicated. With continuous evolution of the detonation front structure, the front shows obvious features of the spinning mode, as shown in Figure 18 at $t = 52.82 - 54.97$. so, this detonation can eventually trigger spinning detonations. By the maximum pressure history on the walls it can be seen that, before the spinning mode is formed, detonation is in the rectangular mode at the early stage, and obvious slapping waves appear on the walls. Then

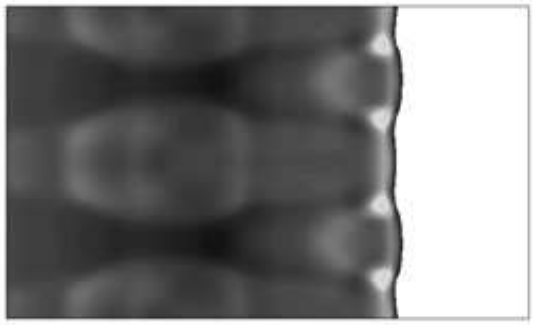

a)

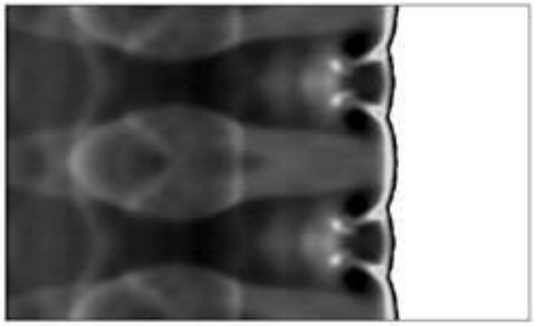

b)

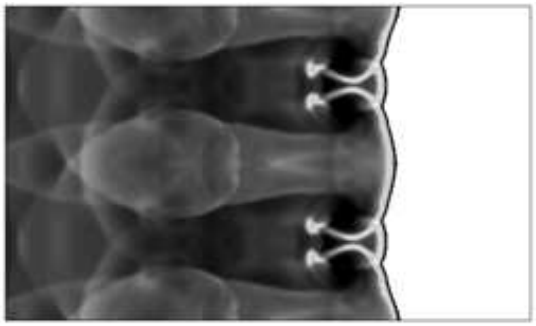

c)

Figure 17: Grid resolution: a) $5pts/L_{1/2}$, b) $10pts/L_{1/2}$, c) $20pts/L_{1/2}$.

the detonation enters a low velocity and low pressure stage for a long time. At last, on the location at about $x = 124.8$, detonation reappears, and the trajectories of the triple lines on the walls become irregular,as shown in Figure 19 (c).

(2) The detonation structure under symmetrical perturbation along the diagonal direction

- Stable detonation ($Ea = 20.0,\ Q = 2.0,\ f = 1.1$)

Figure 20 records the maximum pressure history of detonations on the walls. It can be seen that the slapping waves on the walls disappear. This phenomenon is in agreement with the result in [24]. It is worth noting that, along the propagation direction of detonations, the cell size on the walls increases. Such phenomenon was not observed in [24]. The ratio between the cell width on the walls ($x = 28.8 - 48.0$) in Figure 20 (b) and the one measured in Figure 12 is about 0.7, which is in agreement with the result in [24]. Figure 21 (a,b,c,d) displays the typical diagonal structure of the detonation front, which is in good agreement with the structure in [24]. It can be seen that, moving along the diagonal direction, triple lines do not collide perpendicularly with the walls. So, no slapping waves appear on the walls. Over time, detonation waves still propagate in the diagonal mode, but the triple lines on the front collide, coalesce and form the front structure as shown in Figure 21 (e,f). Because the triple lines coalesce and the number of triple lines moving along the diagonal direction decreases, the cycle for the same pair of triple lines to collide will increase in time. The cell size eventually increases, as shown in Figure 20 (a). Therefore, for stable detonations, the detonations propagate in an in-phase diagonal mode, and the front maintains a diagonal structure.

- Mildly unstable detonation ($Ea = 50.0,\ Q = 50.0,\ f = 1.6$)

Figure 22 shows the front structure at different times. It can be seen that the detonation wave propagates in the diagonal mode at the early stage. At $t = 32.24$, the front becomes an irregular structure. Over time, the front displays a structure featuring spinning detonations.

- Highly unstable detonation ($Ea = 50.0,\ Q = 50.0,\ f = 1.2$)

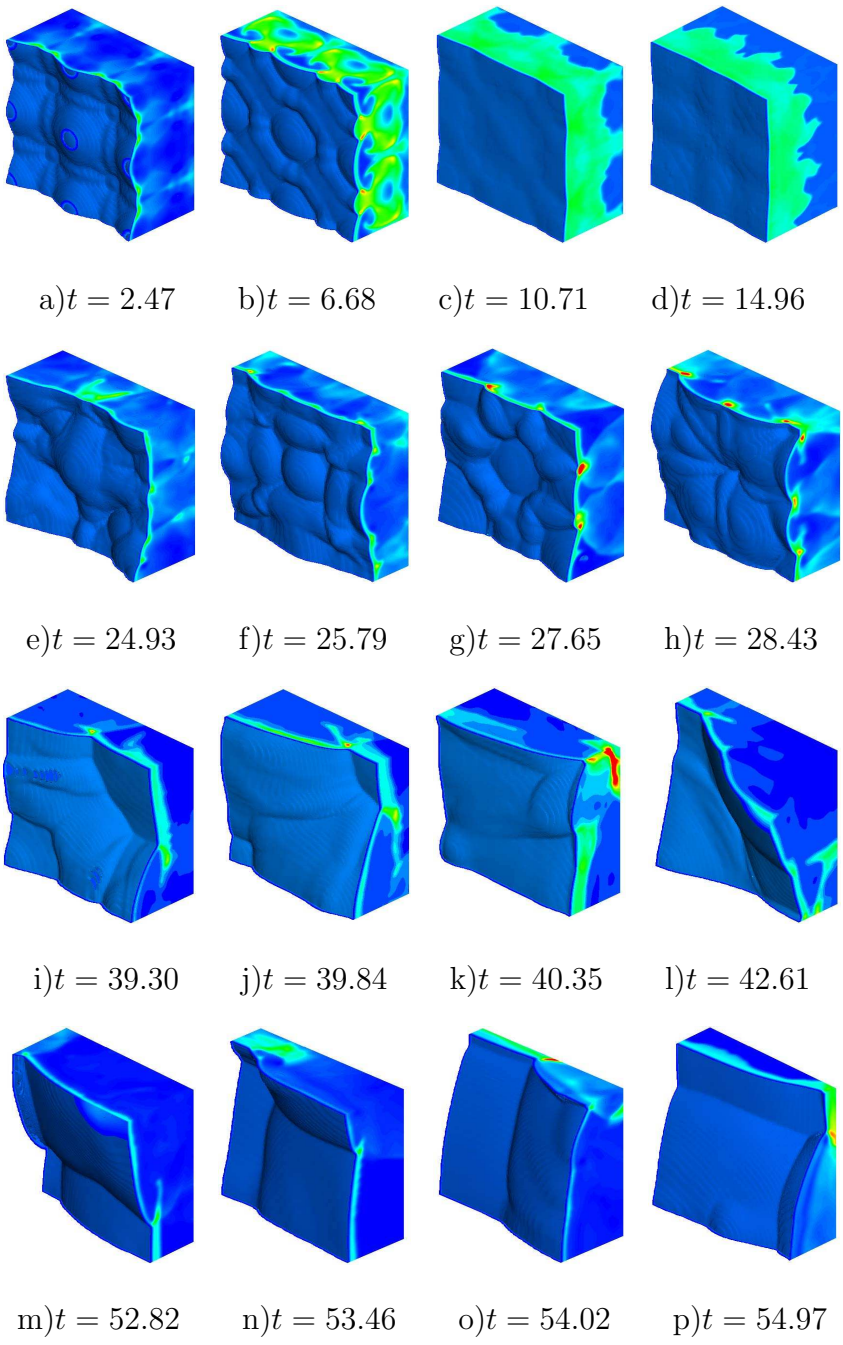

Figure 18: Front structure and density gradient on the walls at different times.

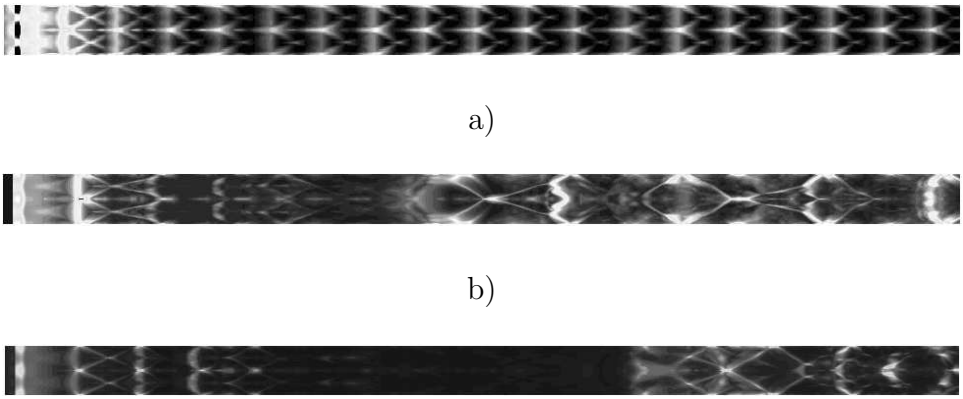

a)

b)

c)

Figure 19: Maximum pressure histories on the wall $y = 0$: a) $Ea = 20.0$,$Q = 2.0$, $f = 1.1$, b) $Ea = 50.0$, $Q = 50.0$, $f = 1.6$, c) $Ea = 50.0$, $Q = 50.0$, $f = 1.2$.

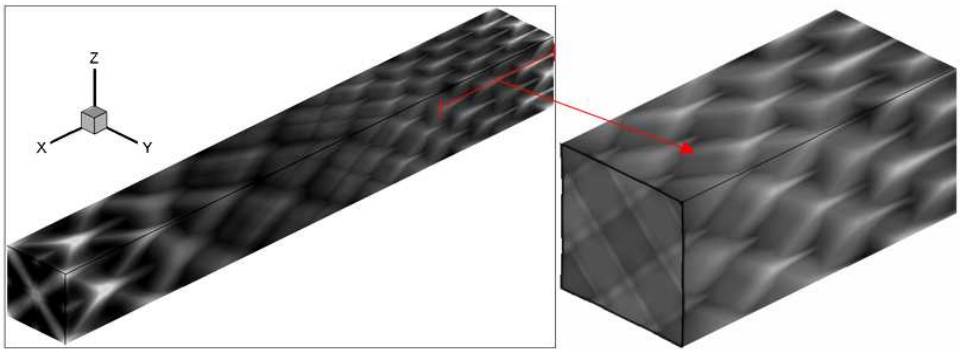

a) b)

Figure 20: Maximum pressure history on the walls: b) is a magnified picture of the cellular structure indicated by the red line in a).

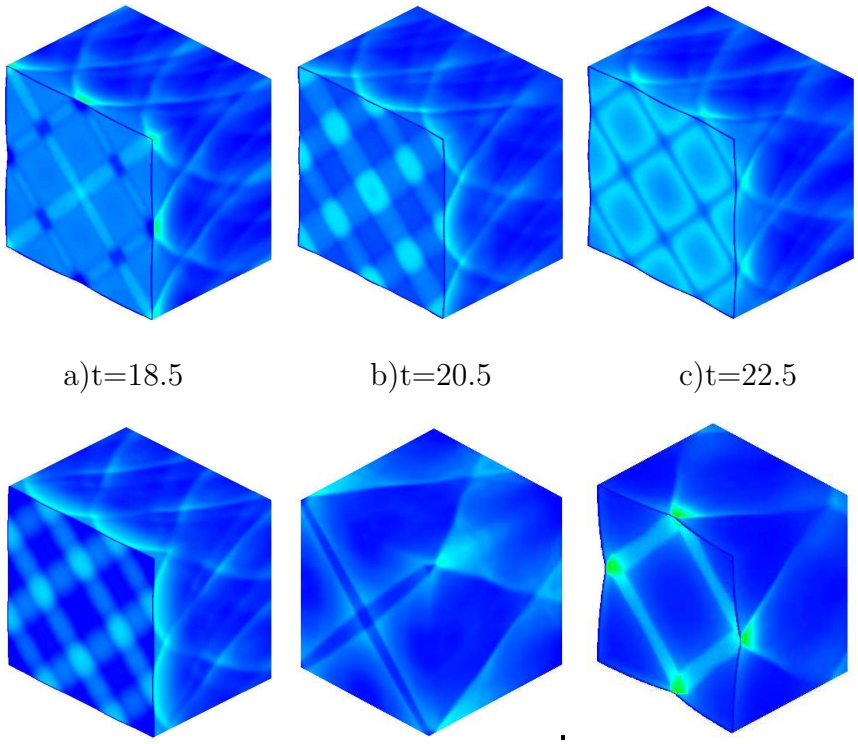

a)t=18.5 b)t=20.5 c)t=22.5

d)t=24.5 e)t=30.5 f)t=34.5

Figure 21: Front structure and pressure gradient on the walls.

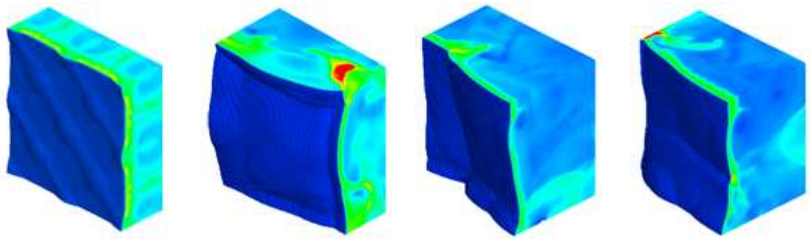

a)$t = 3.82$ b)$t = 32.24$ c)$t = 53.68$ d)$t = 72.71$

Figure 22: Front structure at different times.

Figure 23 displays the evolution process of the front structure at different times. It can be seen from the figure that, at $t = 5.08$, the triple lines move along the diagonal direction, and they collide at the main diagonal (TL1) and the second main diagonal (TL2). The detonation front is very thin and shows a diagonal structure. The triple line shape is shown in Figure 23 (b). At $t = 7.80$, the triple lines collide on the central line between TL1 and TL2. The front structure is shown in Figure 23 (e). At $t = 8.06$, the front becomes flat and thick, the reaction is incomplete, and the detonation velocity decreases. At $t = 66.83 - 71.34$, the front structure is simplified as the features shown in Figure 24 (c-j). At $t = 66.83$, the front is composed of three Mach stems and one incident wave. As the incident waves advance, triple lines move at the direction as shown in Figure 24 (c). At $t = 67.48$, the triple lines are located on the walls. So, the front is also composed of two Mach stems, which is in agreement with the result in [36]. The transverse waves collide with the walls and are reflected, and the triple lines move downward. At $t = 68.13$, the front structure is shown in Figure 23 (k), and the triple lines move at the direction as shown in Figure 24 (e). Hence, for highly unstable detonation, under symmetrical initial perturbation along the diagonal direction, detonations propagate in the in-phase diagonal mode at the early stage, and the front has a diagonal structure. Over time, the diagonal structure of the front breaks down, the front shows a structure featuring spinning detonations, and the detonations show a transition from the diagonal mode to the spinning mode. In Figure 25, the measured spinning angle is 50.2°, and the pitch-to-diameter ratio is 3.15. These are very close to the theoretical values [51]and numerical results [39].It is thus seen that, the critical width for detonations at different chemical reaction parameters triggering spinning mode is different. For the highly unstable detonation, when the duct width is $9.6 \times L_{1/2}$, detonation can still evolve into the spinning mode. For a unstable detonation ($Ea = 50.0$, $Q = 50.0$ and $f = 1.0$), a spinning structure cannot be triggered in a duct with width larger than $4.5 \times L_{1/2}$ (as shown in Figures 5, 7, 8).

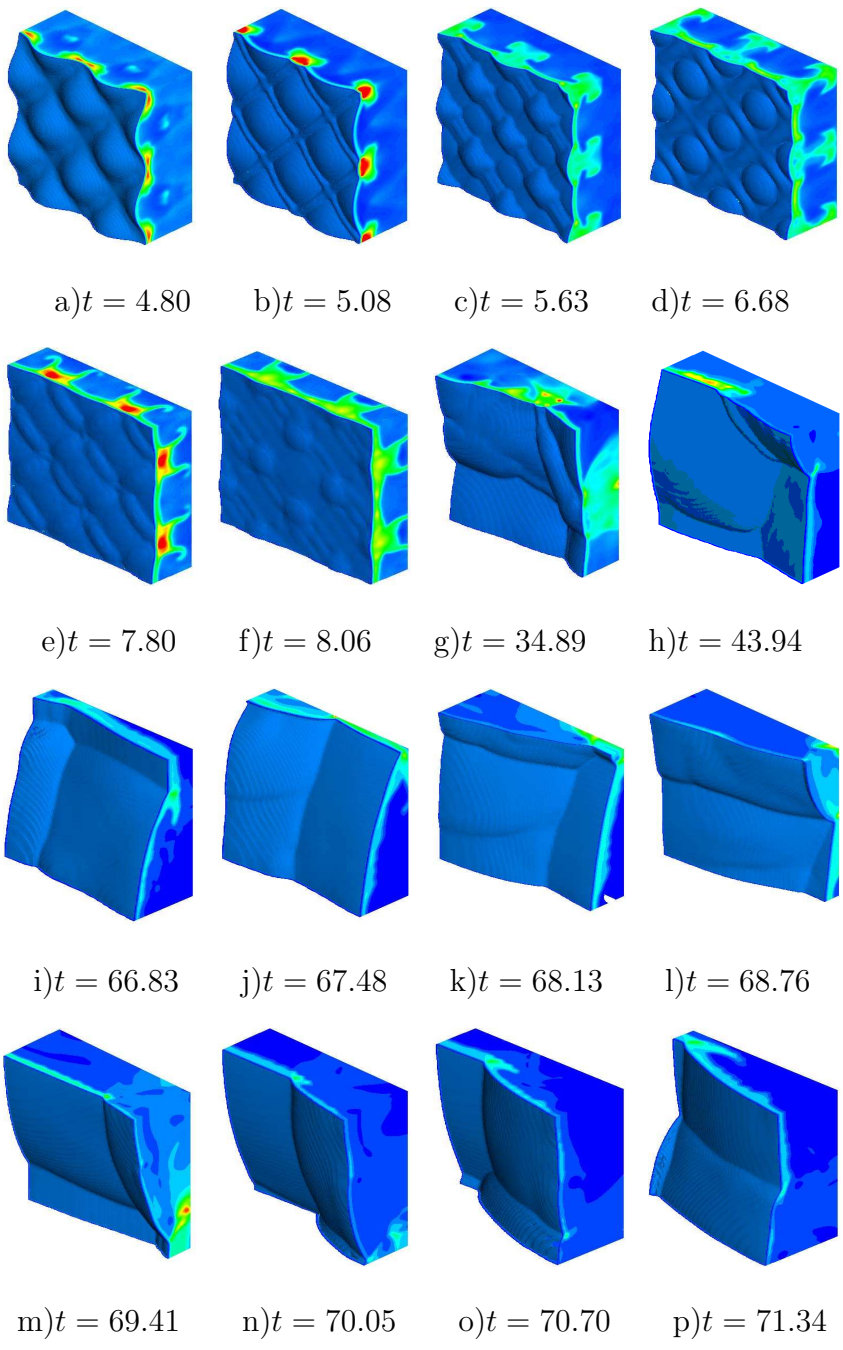

a)$t = 4.80$ b)$t = 5.08$ c)$t = 5.63$ d)$t = 6.68$

e)$t = 7.80$ f)$t = 8.06$ g)$t = 34.89$ h)$t = 43.94$

i)$t = 66.83$ j)$t = 67.48$ k)$t = 68.13$ l)$t = 68.76$

m)$t = 69.41$ n)$t = 70.05$ o)$t = 70.70$ p)$t = 71.34$

Figure 23: Front structure at different times.

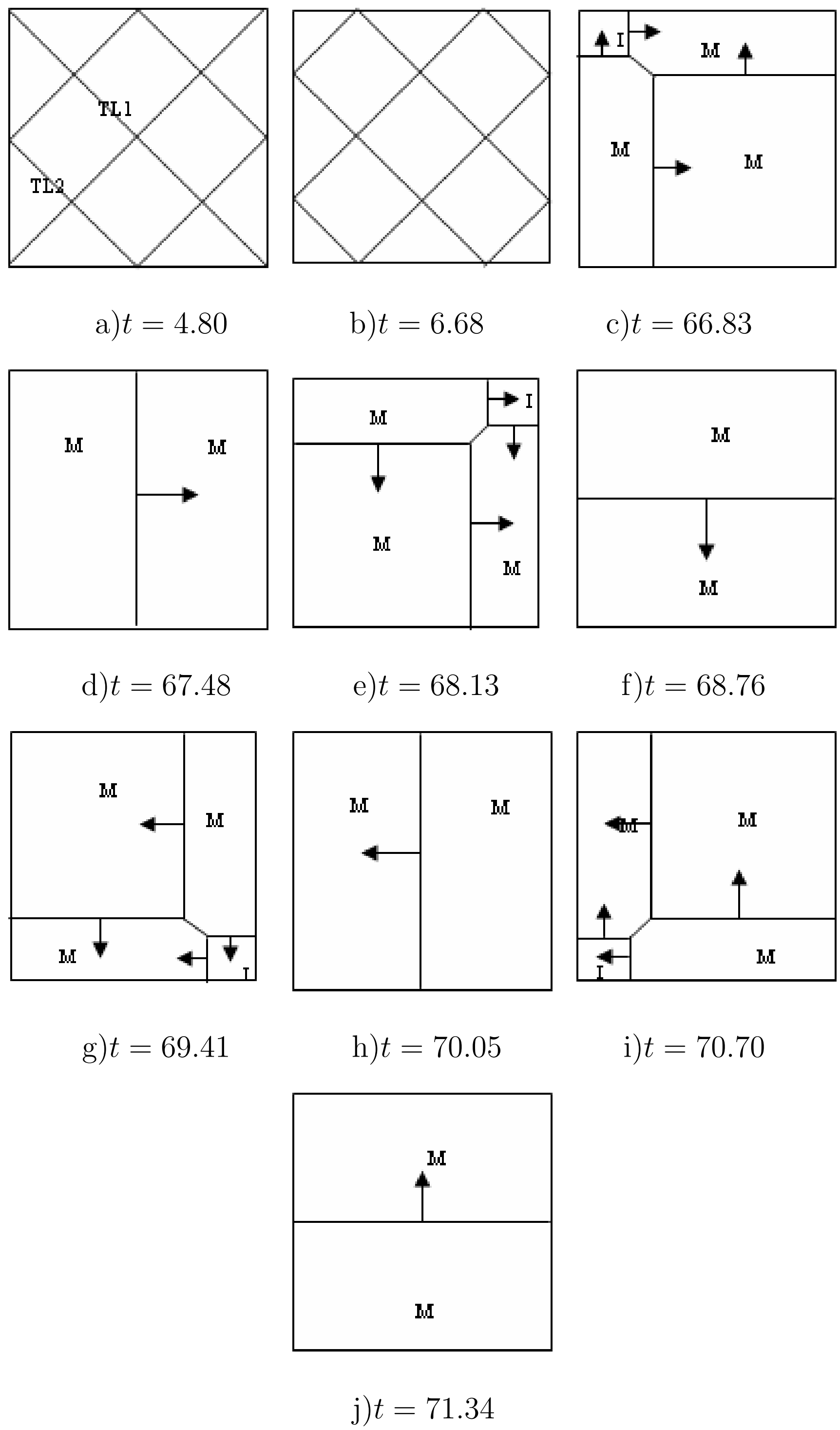

a)$t = 4.80$ b)$t = 6.68$ c)$t = 66.83$

d)$t = 67.48$ e)$t = 68.13$ f)$t = 68.76$

g)$t = 69.41$ h)$t = 70.05$ i)$t = 70.70$

j)$t = 71.34$

Figure 24: Schematic of the spinning detonation front structure: TL1 is the main diagonal triple line, TL2 is the second main diagonal triple line. I is incident wave, M is "Mach leg".

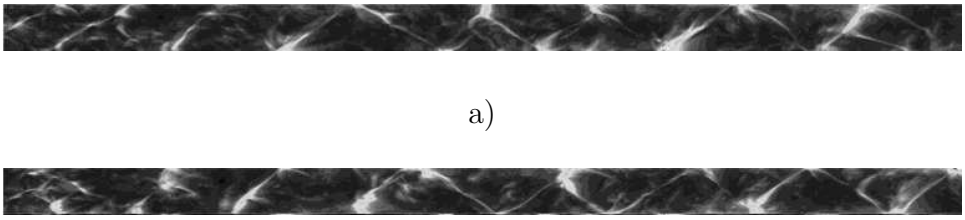

a)

b)

Figure 25: Maximum pressure history on the walls: a) $y = 0.0$, b) $z = 0.0$.

5 Concluding remarks

Using the high-resolution fifth order WENO scheme with third order TVD-Runge-Kutta temporal discretization, we perform extensive numerical simulation for the propagation modes of three-dimensional gaseous detonation front structure in long, straight and rectangular ducts with different width and under different initial perturbations. The following conclusions are reached: (1) Under a transverse sinusoidal perturbation, when the duct width is smaller than the cellular width ($4.5\times L_{1/2}$), the unstable detonation can trigger the spinning mode in the duct. The detonation wave propagates in a single-headed spinning mode, and the ribbon features of single-headed spinning detonations are shown on the walls. The measured pitch-to-diameter ratio is about 3.42, which is a little larger than the theoretical value 3.128. When the duct width is larger than the cellular width, the detonation transitions to an out-of-phase rectangular mode. (2) Under a transverse cosine perturbation, the stable detonation front has a rectangular structure, obvious slapping waves appear on the walls, and the measured cellular width-length ratio is about 0.50. The mildly unstable detonation front has a rectangular structure at the early stage. Over time, the front becomes flat, and at last it becomes a rectangular mode. The highly unstable detonation front has a rectangular structure at the early stage, but after a low velocity stage for a long period of time, it reignites and forms detonation, the detonation front becomes very distorted and the detonation becomes unstable. Eventually, the spinning detonation is triggered. (3) Under the symmetrical perturbation along the diagonal of the front, the stable detonation is in an

in-phase diagonal mode, the detonation front maintains a diagonal structure, the slapping waves on the walls disappear, and the measured cell width-length ratio is equal to that in the case of rectangular structures. Mildly unstable detonation and highly unstable detonation fronts have a diagonal structure at the early stage, but such structure is very unstable. After a short period of time, the diagonal structure of the front breaks down and eventually it evolves into a spinning detonation. Therefore, spinning detonation is the ultimate mode of detonation. Triggering spinning detonation is of significance for stable propagation of highly unstable detonations.

Acknowledgments

The research of C. Wang is supported by Program for New Century Excellent Talents in University under grant number NCET-08-0043, NSFC grants 10972040, National Basic Research Program of China (grant No. 2010CB832706 and 2011CB706904), and the Foundation of State Key Laboratory of Explosion Science and Technology (grant No. ZDKT11-01). The research of C.-W. Shu is supported by ARO grant W911NF-11-1-0091 and NSF grant DMS-1112700. The research of J.G. Ning is supported by NSFC grant 11032002.

References

[1] X.-D. Liu, S. Osher and T. Chan, J. Comput. Phys. 115 (1994) 200-212.

[2] G.S. Jiang and C.-W. Shu, J. Comput. Phys. 126 (1996) 202-228.

[3] D.S. Balsara and C.-W. Shu, J. Comput. Phys. 160 (2000) 405-452.

[4] C.-W. Shu, SIAM Review 51 (2009) 82-126.

[5] A. Bourlioux and A.J. Majda, Trans. R. Soc. London Ser. A 350 (1995) 29-68.

[6] G.J. Sharpe, J. Fluid Mech. 447 (2001) 31-51.

[7] A. Bourlioux, A.J. Majda and V. Roytburd, SIAM J. Appl. Math. 51 (1991) 303-343.

[8] M.V. Papalexandris, A. Leonard and P.E. Dimotakis, J. Comput. Phys. 134 (1997) 31-61.

[9] X. He and A.R. Karagozian, J. Sci. Comput. 19 (2003) 201-224.

[10] Y. Daimon and A. Matsuo, Phys. Fluids 15 (2003) 112-122.

[11] R.H. Guirguis, E.S. Oran and K. Kailasanath, Symposium (International) on Combustion 21 (1988) 1659-1668.

[12] A. Bourlioux and A.J. Majda, Combust. Flame 90 (1992) 211-229.

[13] M.V. Papalexandris, A. Leonard and P.E. Dimotakis, Comput. Math. Appl. 44 (2002) 25-49.

[14] V.N. Gamezo, D. Desbordes and E.S. Oran, Combust. Flame 116 (1999) 154-165.

[15] P. Hwang, R.P. Fedkiw, B. Merriman, T.D. Aslam, A.R.Karagozian and S.J. Osher, Combust. Theor. Model. 4 (2000) 217-240.

[16] J.E. Shepherd, F. Pintgen, J.M. Austin and C.A. Eckett, AIAA 40th Aerospace Sciences Meeting, January 2002. AIAA-2002-0773. Revised January 25, 2002.

[17] D.R. White and K.H. Cary, Phys. Fluids 6 (1963) 749-750.

[18] R.A. Strehlow, Astronaut. Acta. 15 (1970) 345-357.

[19] R. Deiterding and G. Bader, High-resolution simulation of detonations with detailed chemistry. In: Warnecke, G. (ed.), Analysis and Numerics for Conservation Laws 2005, 69-91.

[20] H. He, S.T.J. Yu and Z.C. Zhang, AIAA-2005-0229 (2005).

[21] M. Hanana, M.H. Lefebvre and P.J. Van Tiggelen, Shock Waves 11 (2001) 77-88.

[22] D.N. Williams, L. Bauwens and E.S. Oran, Symposium (International) on Combustion 26 (1996) 2991-2998.

[23] N. Tsuboi, S. Katoh and A.K. Hayashi, Proc. Combust. Inst. 29 (2002) 2783-2788.

[24] V. Deledicque and M.V. Papalexandris, Combust. Flame 144 (2006) 821-837.

[25] C. Campbell and D.W. Woodhead, J. Chem. Soc. (1926) 3010-3021.

[26] F. Zhang and H. Gronig, Phys. Fluids 3(1991) 1983-1990.

[27] J.H. Lee, R.I. Oloukhin and A.K. Oppenheim, Astronaut. Acta. 14 (1969) 565-584.

[28] G.L. Schott, Phys. Fluids 8 (1965) 850-865.

[29] K. Ishii and H. Gronig, Shock Waves 8 (1998) 55-61.

[30] F. Zhang, S.B. Murray and K.B. Gerrard, Shock Waves 15 (2006) 313-324.

[31] Z.W. Huang, M.H. Lefebvre and P.J. Van Tiggelen, Shock Waves 10 (2000) 119-125.

[32] T. Mizutani, H. Matsui, H. Sanui and M. Yonekura, J. Loss Prevent. Proc. 14 (2001) 559-565.

[33] O.V. Achasov and O.G. Penyazkov, Shock Waves 11 (2002) 297-308.

[34] A.R. Kasimov and D.S. Stewart, J. Fluid Mech. 466 (2002) 179-203.

[35] T.P. Ivleva and A.G. Merzhanov, Phys. Rev. E 64 (2001) 036218.

[36] N. Tsuboi, M. Asahara, K. Eto and A.K. Hayashi, Shock Waves 18 (2008) 329-344.

[37] K. Eto, N. Tsuboi and A.K. Hayashi, Proc. Combust. Inst. 30 (2005) 1907-1913.

[38] N. Tsuboi and A.K. Hayashi, Proc. Combust. Inst. 31 (2007) 2389-2396.

[39] H.S. Dou, H.M. Tsai, B.C. Khoo and J. Qiu, Combust. Flame 154 (2008) 644-659.

[40] H.S. Dou, H.M. Tsai, B.C. Khoo, J. Qiu, AIAA Paper-2006-1177 2006.

[41] W. Doering, Ann. Phys. 43 (1943) 421-436.

[42] C.-W. Shu and S. Osher, J. Comput. Phys. 77 (1988) 439-471.

[43] H.I. Lee and D.S. Stewart, J. Fluid Mech. 216 (1990) 103-132.

[44] W. Fickett and W.C. Davis,Detonation, University of California Press, Berkeley CA, 1979.

[45] A. Bourlioux, A. J. Majda and V. Roytburd, SIAM J. Appl. Math. 51 (1991) 303-343.

[46] G.J. Sharpe and S. Falle, Combust. Theor. Model. 4 (2000) 557-574.

[47] M.I. Radulescu, G.J. Sharp, J.H.S. Lee, C.B. Kiyanda, A.J. Higgins and R.K. Hanson, Proc. Combust. Inst. 30 (2005) 1859-1867.

[48] H.S. Dou and B.C. Khoo, Shock Waves 20 (2010) 163-173.

[49] A.K. Hayashi, K. Eto, N. Tsuboi, 20th International Colloquium on the Dynamics of Explosions and Reactive Systems (2005) No. 85.

[50] J.A. Fay, J. Chem. Phys. 20 (1952) 942-950.

[51] J.H. Lee,The Detonation Phenomenon, Cambridge University Press 2008.

[52] N. Tsuboi, M. Asahara and K. Eto, In: Proceedings of the 31st Symposium (International) on Combustion. Combustion Institute, Pittsburgh, (2007) 2389-2396.

[53] J.J. Erpenbeck, Phys. Fluids 7 (1964) 684-696.

[54] J.J. Erpenbeck, Phys.Fluids 5(1962)604-615.